THE ASTROPHYSICAL JOURNAL, 196:413–432, 1975 March 1

A PHOTOMETRIC STUDY OF NGC 2419

RENÉ RACINE* AND WILLIAM E. HARRIS†
David Dunlap Observatory, Richmond Hill, Ontario; and Erindale College, University of Toronto
Received 1974 July 11

ABSTRACT

Photometry to $V = 22.2$ and $B = 23.7$ is reported for the outer-halo globular cluster NGC 2419. The color-magnitude diagram of the cluster is similar to that of the classic metal-poor cluster M92, and indicates a very low metallicity $Z \simeq 1.5 \times 10^{-4}$. The reddening $E(B - V)$ is 0.03 ± 0.01 mag, and the apparent distance modulus is $(m - M)_V = 19.87 \pm 0.09$, leading to a galactocentric distance of $R_g = 100 \pm 5$ kpc. The RR Lyrae nature of the numerous short-period variables discovered by Baade is confirmed; of the five known brighter variables, one appears to be a Population II Cepheid, while the others fall near the tip of the red giant branch. Attention is drawn to a significant gap in the giant branch. The cluster's age is estimated as $T = 11.0 \pm 0.5 \times 10^9$ yr from its HB morphology, or $T = 11.9 \pm 0.3 \times 10^9$ yr from a discussion of its galactic orbit.

The galactic orbit of NGC 2419 is determined. The cluster is gravitationally bound to the Galaxy, traveling on an orbit of eccentricity 0.62 with a period of 3.4×10^9 yr, and is presently near its apogalacticon. It is argued that the cluster was born close to its perigalacticon distance of 24 kpc. A possible gravitational encounter between NGC 2419 and the Magellanic Clouds is mentioned briefly. Finally it is shown that NGC 2419, like many metal-poor halo clusters, possesses an orbit of large angular momentum per unit mass h, and that globular clusters with the largest h are among the metal poorest.

Subject headings: galactic structure — globular clusters

I. INTRODUCTION

The northern cluster NGC 2419 (α: 7^h35^m; δ: $+39°00'$ (1950); $l = 180.°4$, $b = +25.°6$) is of interest simply because of its enormous distance. Drifting in intergalactic space at 100 kpc from the center of the Galaxy, this object marks one of the last detectable outposts of our Galactic system. Along with a very few Palomar clusters, NGC 2419 is the most distant globular cluster for which the color-magnitude (C-M) diagram can still be studied in detail.

The C-M diagrams already obtained for "intergalactic" globular clusters like NGC 7006 (Sandage and Wildey 1967) and Pal 3 and 4 (Burbidge and Sandage 1958), and for the dwarf spheroidal galaxies in Draco (Baade and Swope 1961) and Ursa Minor (van Agt 1967), have shown unusual features whose interpretation in terms of abundance peculiarities (Hartwick 1968; Hartwick and McClure 1972) or age differences (Rood 1973) remains problematic. Furthermore, all the known clusters and dwarf spheroidals farther than ~40 kpc from the Galactic center *except* for NGC 2419 are diffuse, low-density objects which could not survive close tidal encounters with the Galaxy. By contrast NGC 2419 is a populous and compact (class II) object similar to the "nearby" common halo globular clusters. Thus an investigation of its stellar population could help to disentangle the effects of galactocentric distance and of space density on the evolutionary characteristics of Population II systems.

II. OBSERVATIONS

NGC 2419 is difficult to observe. Visual inspection under good seeing at the prime focus of the 200-inch telescope shows the brightest cluster stars barely resolved, and crowding problems impose severe limitations on photometric measurements except in the outer regions. The only previously published photometry of the cluster stars in the last 40 years is the work by Baade (1935) on the variables, an eloquent testimony to the observational difficulty presented by this outstanding object.

A local sequence of photoelectric *UBV* standards around the cluster down to $V = 17.1$ was measured with the No. 1 36-inch (91 cm) telescope at the Kitt Peak National Observatory in 1973 January. These standards are identified in figure 1, and their photoelectric and photographically smoothed magnitudes and colors are listed in table 1. For the photoelectric measurements, standard *UBV* filters were used with a 1P21 phototube and single-channel pulse counting equipment. Standard and extinction stars used to transform the instrumental measures to the *UBV* system were taken from Johnson *et al.* (1966), Crawford *et al.* (1971), and the Cerro Tololo list of standards compiled by Demers and Kunkel.

Average values of the standard deviation of a single photoelectric measurement, as judged from the night-to-night scatter of the individual measures, are listed in table 2 as a function of the magnitude level V. The entries in this table should be divided by $\sqrt{n}$ to give the internal standard errors of the photoelectric values in table 1.

* Guest investigator at the Hale Observatories.

† Visiting astronomer 1973, Kitt Peak National Observatory, operated by the Association of Universities for Research in Astronomy, Inc., under contract with the National Science Foundation.

TABLE 1

PHOTOMETRIC DATA FOR STANDARD STARS

Star	V	$B-V$	n	$U-B$	n	V_{pg}	$(B-V)_{pg}$
+39°1979....	7.19	0.27	5	0.07	4	...	...
+39°1978....	7.94	0.15	5	0.07	4	...	...
+39°1976....	9.32	0.34	5	0.08	4	...	...
A...........	11.12	0.87	5	0.47	4	...	...
B...........	11.94	1.09	5	0.95	4	...	...
C...........	12.29	0.59	5	0.08	3	...	...
D...........	13.00	0.50	4	0.02	3	...	...
E...........	13.40	0.51	4	−0.04	3	13.41	0.49
F...........	13.47	0.58	4	−0.01	3	13.46	0.55
G...........	13.51	0.63	5	0.04	3	13.48	0.62
H...........	13.57	1.22	5	1.14	4	13.65	1.19
I...........	13.75	0.67	4	0.17	3	13.73	0.67
J...........	14.33	0.63	4	0.14	3	14.27	0.67
K...........	15.19	0.50	2	−0.06	1	15.31	0.34
L...........	15.24	0.78	5	0.43	4	15.30	0.78
M...........	15.37	0.89	5	0.67	3	15.31	1.02
N...........	15.55	0.59	4	−0.05	3	15.47	0.76
P...........	15.55	0.55	4	0.04	3	15.47	0.63
Q...........	15.74	0.71	2	0.23	1	15.87	0.55
R...........	15.81	0.81	2	0.31:	1	15.69	0.98
S...........	15.82	0.64	5	−0.08	4	15.79	0.64
T...........	15.87	0.78	4	0.23:	2	15.86	0.79
U...........	16.00	0.78	3	0.19	2	16.09	0.66
V...........	16.03	1.03	2	0.76	1	16.16	0.93
W...........	16.13	1.20	4	0.69	2	16.09	1.27
X...........	16.69	0.99	2	0.45:	1	16.70	0.93
Y...........	16.91	0.88	2	0.25:	1	16.92	0.92
Z...........	17.14	1.35	1	...	...	17.10	1.27

TABLE 2

RANDOM ERRORS OF SINGLE PHOTOELECTRIC MEASURES

V	σ_v	σ_{B-V}	σ_{U-B}
<13.0........	0.015	0.014	0.019
13.0–16.0......	0.022	0.034	0.035
>16.0........	0.06	0.06	(0.05)

A series of B and V plates of the cluster was obtained with the 200-inch telescope as described in table 3. These were taken at the prime focus with the f/3.67 Ross corrector, and with an auxiliary calibration wedge described by Racine (1969, 1971). This wedge produces artificial secondary images of each star which are fainter than their primaries by $\Delta m = 5.00$ mag, and which are used to extend the photometric calibration to the plate limit ($V_{\mathrm{lim}} \approx 22.2$, $B_{\mathrm{lim}} \approx 23.7$).

On the six photographic plates, all uncrowded stars within two annular regions north and south of the cluster center (rings A and B, as shown in fig. 1) were measured with a Cuffey-type iris photometer at the David Dunlap Observatory. The east and west sectors containing the bright field star BD+39°1979 and its ghost image were excluded because of obvious background problems. In addition to rings A and B, a few brighter stars were measured within the inner boundary of ring A (called the "inner region") in order to help delineate the upper part of the giant branch of the cluster. All the stars measured photographically are identified in figure 1 (ring B and outer ring A) and figure 2 (inner ring A and inner region).

The color equations for the plate-filter combinations used were known from previous work on M67 (Racine 1971) and were verified from the NGC 2419 standard sequence. The relations between the photographic and photoelectric magnitudes used were

$$V = y + 0.118\,(b - y)\,, \qquad (1a)$$

$$B = b - 0.064\,(b - y)\,. \qquad (1b)$$

TABLE 3

JOURNAL OF PHOTOGRAPHIC OBSERVATIONS

Plate No.	Date	PST	Emulsion+Filter	Exposure (minutes)
PH-5461-R....	1970 Apr. 4	07:20	103aO+GG13	20
PH-6167-R....	1972 Mar. 9	07:41	103aD+GG11	30
PH-6168-R....	1972 Mar. 9	08:14	103aD+GG11	30
PH-6169-R....	1972 Mar. 9	08:43	103aO+GG13	20
PH-6170-R....	1972 Mar. 10	07:20	103aO+GG13	20
PH-6175-R....	1972 Mar. 10	09:09	103aO+GG13	20

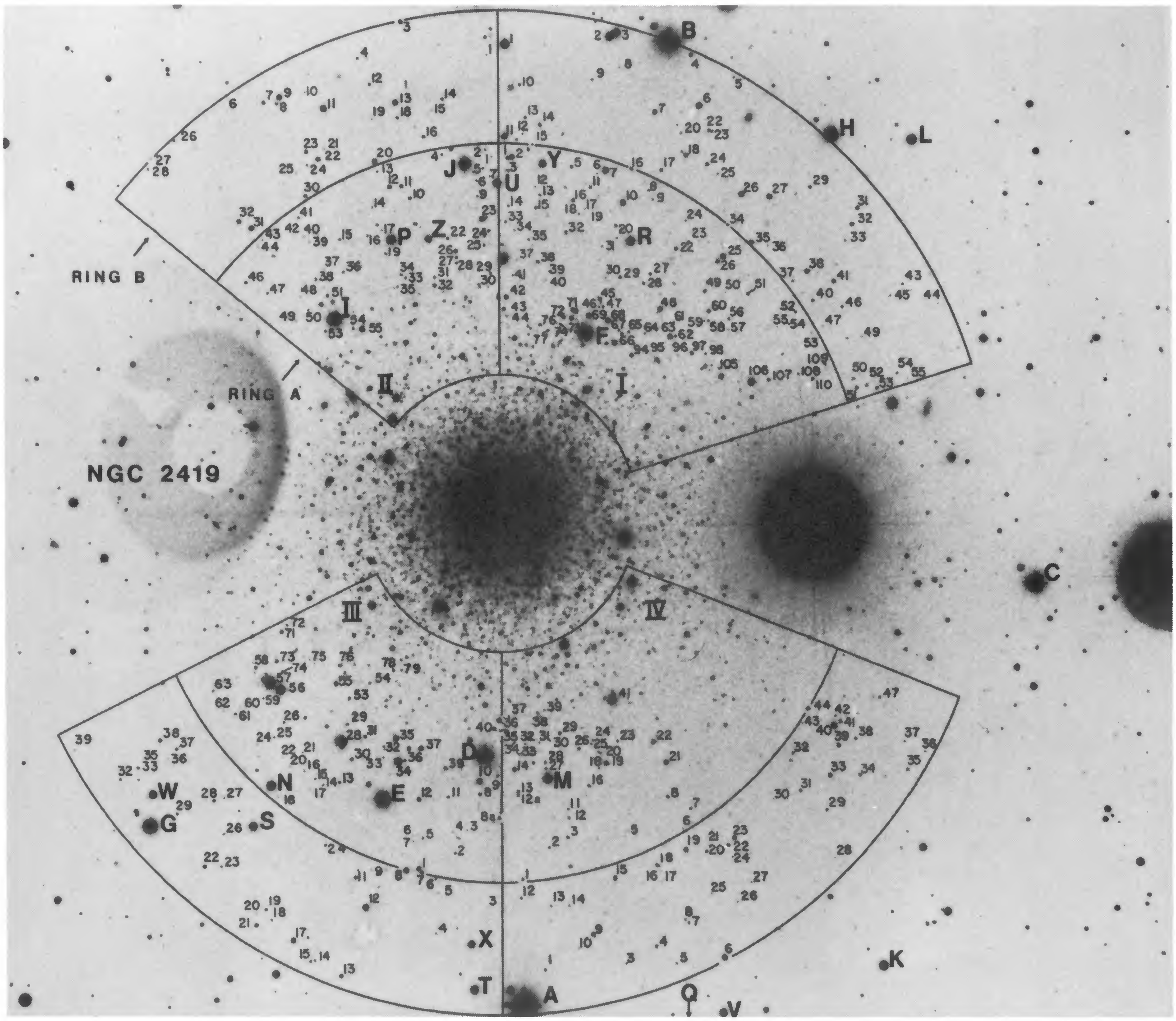

FIG. 1.—Finder chart for the photometric survey of NGC 2419, made from a 30-min V exposure at the prime focus of the 200-inch. North is at the top and east at left. The photoelectrically measured standard stars are marked by capital letters, and their secondary images appear 15″ NE of each one. The region measured photographically is divided into two annular rings, A and B, and four sectors I–IV as shown. The three concentric circles defining rings A and B have radii of 1′.69, 4′.50, and 6′.13. The photographically measured program stars are shown for ring B and the outer part of ring A; wherever possible, the number is placed to the right of the star. At left, the shadows of the "auxiliary wedge" and its holder can be seen in the out-of-focus ghost image of the bright star BD+39°1979.

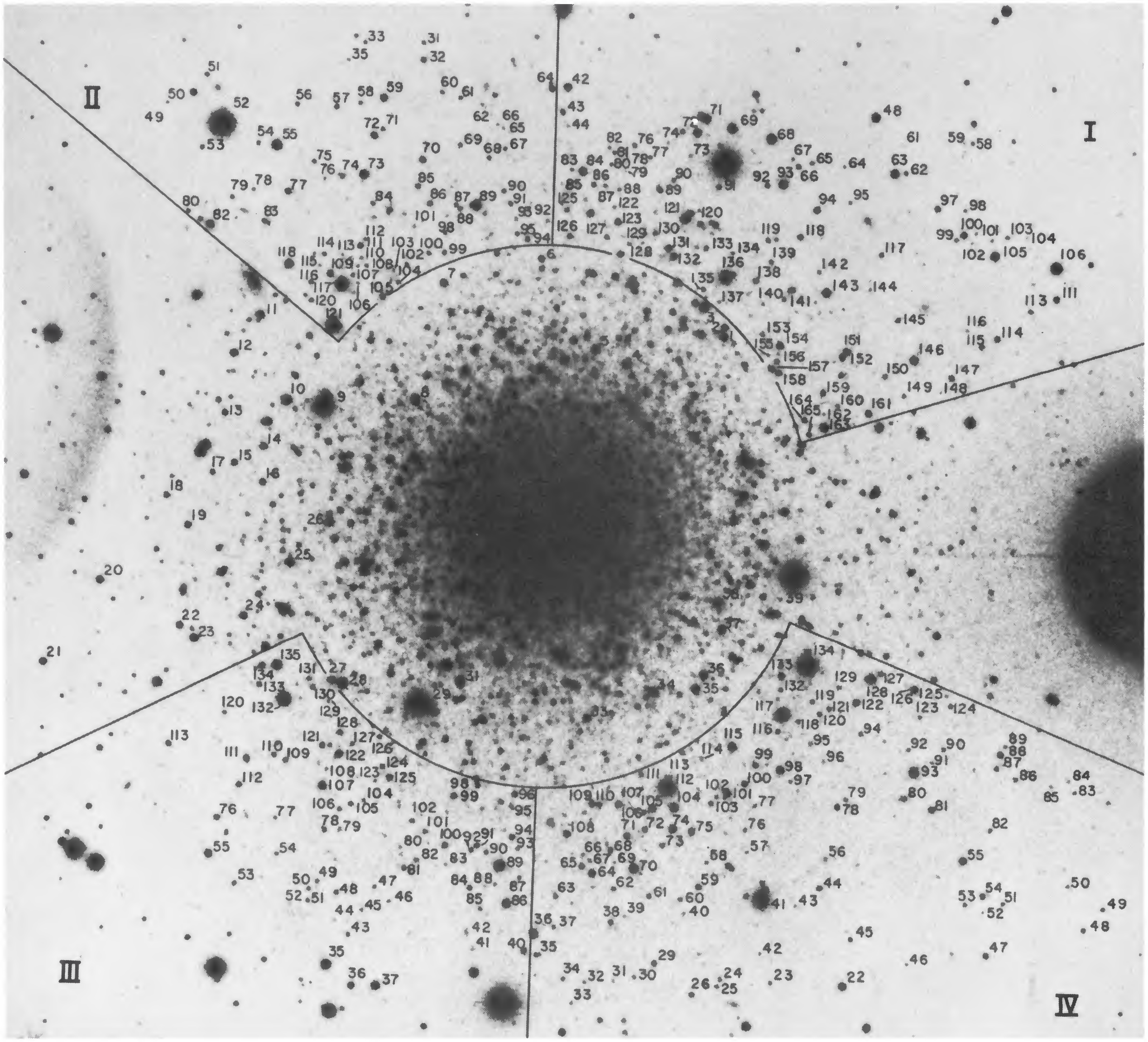

FIG. 2.—Finder chart for the program stars in the inner part of ring A and in the "inner region" around the cluster center

TABLE 4

NGC 2419—Program Stars Ring A

STAR	V	B−V	STAR	V	B−V	STAR	V	B−V	STAR	V	B−V	STAR	V	B−V	STAR	V	B−V
I 1	19.44	0.54	54	21.42	0.44	107	19.87	0.72	159	19.87	0.12	50	21.13	0.72	105	20.55	0.15
2	17.88	0.44	55	22.25	0.59	108	21.31	0.21	160	20.81	0.47	51	20.12	0.90	106	21.43	0.90
3	20.52	0.21	56	20.76	0.58	109	20.68	0.56	161	19.02	0.90	53	20.23	0.30	107	20.50	0.19
5	20.36	0.71	57	22.05	0.26	110	20.19	0.71	162	21.39	0.56	54	20.53	0.81	108	20.93	0.88
6	22.00	0.64	58	20.86	−0.08	111	19.52	1.21	163	18.07	0.96	55	17.58	0.58	109	21.30	0.93
7	17.26	0.89	59	21.97	0.26	113	20.35	0.19	164	19.76	0.69	56	20.47	0.11	110	21.16	0.93
8	21.35	0.64	60	19.61	0.82	114	19.59	0.80	165	20.13	0.70	57	20.07	0.82	111	19.51	0.85
9	21.78	0.46	61	21.86	0.63	115	20.06	0.44	II 1	21.78	−0.13	58	20.83	0.77	112	20.86	0.57
10	17.81	1.09	62	20.48	0.07	116	21.51	0.40	2	21.56	1.74	59	18.81	0.97	113	21.48	0.53
11	20.86	1.64	63	18.39	0.94	117	20.40	1.60	4	21.11	1.04	60	20.74	0.69	114	20.42	0.34
12	21.76	0.51	64	21.38	0.71	118	19.76	0.80	5	21.28	0.50	61	20.86	0.94	115	21.55	0.70
13	20.67	−0.05	65	20.87	1.01	119	20.08	0.48	6	21.07	0.91	62	21.35	0.91	116	19.19	0.96
14	21.49	0.62	66	19.96	0.76	120	19.65	0.77	7	21.46	0.90	64	19.40	0.93	117	16.48	1.43
15	20.65	0.82	67	21.52	0.45	121	17.58	1.21	9	21.66	−0.09	65	21.71	1.39	118	18.13	1.07
16	20.02	0.75	68	17.90	1.10	122	21.53	0.75	10	20.22	0.87	66	21.73	1.25	120	20.49	0.74
17	22.06	0.51	69	17.89	1.10	123	19.28	0.93	11	19.13	0.46	67	20.66	0.11	121	15.93	0.93
18	21.75	0.49	71	18.16	0.51	125	20.49	0.16	12	19.02	0.95	68	20.54	0.12	IIII	18.44	0.85
19	22.31	0.10	72	19.98	0.59	126	19.68	0.86	13	21.48	0.61	69	20.70	0.78	2	21.36	2.14
20	21.81	0.83	73	21.38	0.65	127	20.57	0.74	14	21.73	0.07	70	19.43	0.86	3	21.77	0.67
22	19.58	0.88	74	21.89	0.48	128	19.29	0.84	15	21.26	0.75	71	20.43	0.11	4	21.59	1.04
23	21.00	0.77	76	20.35	0.19	129	21.05	0.84	16	21.66	1.58	72	19.07	0.93	5	21.58	0.43
24	21.70	1.08	77	20.83	0.82	130	20.36	0.90	17	21.85	0.48	73	18.18	0.51	6	22.47	1.25
25	17.76	1.16	78	22.04	1.07	131	18.96	0.92	19	20.77	0.69	74	20.35	0.73	7	22.09	0.73
26	19.36	1.51	79	22.03	0.81	132	18.81	0.91	22	20.38	0.33	75	20.48	0.19	8	19.82	0.52
27	20.53	0.83	80	21.14	0.83	133	20.40	0.64	23	18.05	1.11	76	21.50	1.22	8A	19.80	0.73
28	20.60	0.79	81	20.63	0.04	134	20.95	0.77	24	20.36	0.53	77	19.38	0.99	9	20.58	0.80
29	20.44	0.80	82	21.15	0.59	135	20.45	0.21	25	20.66	0.16	78	21.07	0.79	10	17.54	1.29
30	22.06	0.41	83	21.08	0.76	136	16.30	0.91	26	19.36	0.85	79	20.53	0.07	11	20.94	0.81
31	21.77	0.62	84	18.52	0.97	137	21.19	0.77	27	20.22	0.79	80	20.21	0.89	12	18.97	0.87
32	20.56	0.79	85	21.83	0.64	138	20.15	1.06	28	20.71	0.17	82	19.22	1.75	13	20.42	1.56
33	21.19	0.28	86	20.13	0.70	139	20.34	0.21	29	20.61	0.14	83	20.02	0.53	14	21.23	0.58
34	21.92	0.29	87	20.59	0.05	140	21.56	0.58	30	20.65	0.10	84	20.57	0.81	15	21.13	0.89
35	21.35	0.87	88	21.22	0.79	141	20.58	0.08	31	20.70	0.06	85	20.11	0.84	16	21.86	0.41
37	22.05	1.31	89	19.59	0.86	142	20.87	0.79	32	19.81	0.94	86	20.07	0.89	17	22.47	0.59
38	19.82	0.80	90	20.60	0.67	143	18.38	1.33	33	20.59	0.19	87	20.56	0.65	18	22.04	1.04
39	20.42	0.19	91	19.81	0.63	144	21.25	0.73	34	20.41	0.18	88	20.40	0.16	20	22.06	0.07
40	22.04	0.28	92	20.04	0.74	145	20.29	0.10	35	21.48	0.77	89	17.56	0.61	21	21.62	0.74
41	21.78	0.37	93	18.15	1.38	146	18.31	0.93	36	20.59	0.20	90	20.60	0.81	22	22.38	−0.37
42	18.92	0.90	94	19.25	1.27	147	19.56	0.71	37	22.60	0.87	91	20.60	0.22	24	22.21	1.35
43	19.95	0.85	95	21.03	−0.03	148	21.75	0.56	38	20.78	0.14	92	21.35	0.87	25	21.35	0.95
44	21.69	0.55	97	19.57	0.79	149	20.66	0.02	39	22.06	0.29	93	21.45	0.84	26	20.92	1.27
45	19.08	0.92	98	21.48	0.39	150	20.33	0.00	40	22.24	0.67	94	20.23	0.40	28	14.84	0.39
46	21.07	0.00	99	20.89	0.70	151	18.73	0.93	41	21.79	0.80	95	20.64	0.14	29	20.88	0.78
47	20.43	0.14	100	19.19	0.92	152	19.15	0.77	42	22.08	0.51	98	20.72	0.16	30	19.86	0.71
48	18.19	1.01	101	21.41	0.70	153	20.42	0.20	43	21.67	1.65	99	20.59	0.65	31	19.93	0.86
49	19.91	0.59	102	21.93	0.25	154	18.70	0.93	44	22.39	0.60	100	20.61	0.14	32	21.55	0.68
50	22.07	0.57	103	21.33	0.68	155	21.11	0.59	46	20.43	0.88	101	21.54	0.56	33	21.27	0.68
51	20.50	0.65	104	20.86	0.84	156	19.79	0.68	47	21.03	0.73	102	20.75	0.70	34	16.20	0.82
52	20.84	0.79	105	18.23	1.04	157	19.37	0.76	48	22.19	0.87	103	21.45	0.71	35	17.66	0.56
53	22.22	0.55	106	17.05	0.60	158	19.06	0.83	49	21.99	0.94	104	20.59	0.61	36	19.06	1.01

TABLE 4—*Continued*

STAR	V	B−V	STAR	V	B−V	STAR	V	B−V
37	18.36	1.01	96	19.98	0.64	23	20.94	0.86
39	19.62	0.85	98	19.96	0.61	24	20.87	0.04
40	19.44	0.82	99	19.63	0.83	25	20.76	−0.01
41	21.64	−0.20	100	19.71	0.82	26	19.96	0.82
42	21.25	0.67	101	20.50	0.18	27	20.63	0.04
43	20.74	0.00	102	20.69	0.71	28	20.75	0.69
44	22.00	0.62	104	21.10	0.78	29	20.18	0.78
45	21.54	0.71	105	20.18	0.13	30	21.24	0.45
46	21.35	0.51	106	20.58	0.18	31	21.97	0.34
47	21.08	0.70	107	18.37	1.04	32	21.42	0.70
48	20.45	0.74	108	21.19	0.80	33	21.67	0.65
49	20.80	0.76	109	20.17	0.79	34	20.79	0.10
50	20.60	0.11	110	20.03	0.85	35	20.32	0.48
51	20.82	1.40	111	19.16	0.93	36	18.47	1.10
53	20.47	0.78	112	19.65	1.52	37	20.78	0.14
54	21.22	0.80	113	19.83	0.78	38	20.25	0.72
55	18.60	1.02	120	20.75	0.37	39	22.00	0.25
56	15.32	0.65	121	19.53	0.78	40	21.80	0.71
57	14.65	0.90	122	18.70	0.98	41	15.60	0.64
58	21.76	0.52	123	21.38	0.63	42	21.76	0.71
59	21.23	1.02	124	20.01	0.76	43	21.89	0.44
60	22.24	1.60	125	19.28	0.93	44	19.99	0.75
61	20.78	0.08	126	20.33	0.31	45	20.39	0.68
62	22.37	1.53	127	20.55	0.16	46	21.50	0.62
63	20.87	0.64	128	19.89	0.79	47	19.75	0.76
71	19.45	0.60	129	21.07	0.69	48	20.51	0.60
72	20.63	0.19	130	20.03	0.76	49	20.70	1.37
73	19.50	0.78	131	20.68	0.62	50	21.43	0.68
74	20.60	0.02	132	16.27	0.74	51	20.94	0.63
75	21.55	0.86	133	19.94	0.81	52	21.92	0.39
76	19.73	0.82	134	19.18	0.89	53	20.78	0.00
77	21.30	0.75	135	17.72	0.47	54	19.92	0.74
78	20.27	0.21	IV 1	20.82	0.02	55	19.02	0.88
79	20.99	0.54	2	20.90	0.76	56	21.11	−0.09
80	21.63	0.73	3	20.53	0.15	57	21.56	0.61
81	19.97	0.35	5	22.28	0.92	58	21.32	0.92
82	20.61	0.85	6	23.09	0.85	59	19.89	1.63
83	21.60	0.68	7	20.67	0.60	60	20.66	0.12
84	19.98	0.84	8	20.57	0.70	61	20.44	0.11
85	20.93	0.84	11	21.91	0.87	62	20.61	0.72
86	18.29	1.02	12	20.95	0.63	63	20.71	0.80
87	20.78	0.06	12A	20.67	0.72	64	19.09	0.92
88	21.49	0.67	13	19.80	0.69	65	19.70	0.80
89	17.33	1.34	14	18.96	0.95	66	21.56	0.53
90	20.53	0.10	16	20.43	0.13	67	20.92	0.62
91	20.16	0.68	18	21.70	0.71	68	20.12	0.51
92	20.49	0.16	19	18.34	1.43	69	21.60	0.76
93	21.43	0.69	20	21.62	0.84	70	18.07	1.24
94	19.95	0.85	21	18.44	0.98	71	19.64	0.79
95	20.91	0.06	22	18.67	0.81	72	20.07	0.76

STAR	V	B−V	STAR	V	B−V	STAR	V	B−V
73	20.53	0.81	93	17.86	1.13	113	20.56	0.12
74	18.72	0.95	94	20.70	0.60	114	21.61	0.70
75	19.55	0.44	95	21.01	0.68	115	18.50	0.95
76	20.99	0.13	96	21.71	0.56	116	20.29	0.32
77	21.18	0.84	97	21.28	0.81	117	16.46	1.04
78	19.82	0.78	98	18.69	0.93	118	20.51	0.09
79	20.96	0.78	99	19.68	1.47	119	20.46	0.16
80	20.32	1.49	100	19.74	0.79	120	20.27	0.62
81	19.44	0.81	101	18.54	0.93	121	20.18	0.25
82	20.81	0.68	102	20.98	0.76	122	19.09	0.91
83	21.40	0.59	103	20.42	0.19	123	21.02	0.62
84	21.50	0.86	104	18.25	1.00	124	20.23	0.44
85	21.58	0.27	105	19.05	0.94	125	21.39	0.70
86	20.49	0.01	106	20.52	0.15	126	18.78	0.88
87	20.31	0.06	107	19.29	0.90	127	19.90	0.71
88	19.26	0.84	108	19.33	0.92	128	17.84	1.12
89	20.95	0.39	109	19.24	0.86	129	20.66	0.75
90	20.60	0.04	110	20.03	0.82	132	20.57	0.14
91	21.36	0.51	111	20.45	0.79	133	19.10	0.91
92	20.91	0.73	112	15.60	0.87	134	14.73	1.01

NGC 2419 – PROGRAM STARS INNER REGION

STAR	V	B−V	STAR	V	B−V	STAR	V	B−V
1	18.35	1.05	13	19.33	0.93	25	18.05	1.08
2	18.70	1.04	14	18.93	1.00	26	17.81	1.11
3	17.54	1.36	15	19.28	0.80	27	18.62	0.76
4	17.76	1.21	16	19.23	0.88	28	17.30	1.38
5	17.68	1.23	17	20.00	0.53	29	13.85	1.00
6	19.14	1.01	18	19.48	0.77	31	17.78	1.22
7	18.84	1.03	19	18.99	0.92	33	18.32	1.03
8	17.43	1.40	20	18.64	1.07	34	17.45	1.11
9	14.50	0.59	21	18.64	0.96	35	18.25	1.06
10	17.59	1.28	22	18.92	0.94	36	18.14	1.13
11	18.25	1.09	23	18.14	0.54	37	18.16	1.13
12	18.63	0.99	24	18.63	0.91	38	17.43	1.33
						39	13.45	0.79

TABLE 4—*Continued*

NGC 2419—PROGRAM STARS RING B

STAR	V	B−V	STAR	V	B−V	STAR	V	B−V
I 1	15.74	0.76	4	20.89	0.86	32	20.76	0.10
2	16.01	0.89	6	21.99	0.51	33	20.30	0.87
3	16.02	1.03	7	19.68	1.44	35	22.09	0.18
4	19.21	0.92	8	20.58	0.12	36	21.86	0.62
5	21.64	0.19	9	17.61	0.36	37	20.34	0.68
6	17.52	0.64	10	21.77	0.72	38	19.36	0.77
7	18.72	1.32	11	16.95	0.51	39	21.38	−0.07
8	21.76	−0.34	12	20.72	0.18	IV 1	20.92	0.74
9	21.48	0.16	13	17.80	1.07	3	21.51	0.90
10	20.70	0.13	14	20.72	0.06	4	20.76	1.71
11	17.31	0.93	15	22.19	1.48	5	21.41	0.82
12	21.07	0.80	16	20.28	0.82	6	17.69	1.25
13	20.77	1.14	18	20.54	0.17	7	20.89	0.70
14	19.99	1.52	19	21.82	1.18	8	21.21	0.84
15	21.26	0.67	20	18.16	1.57	9	18.94	1.46
16	20.14	0.96	21	21.80	1.46	10	21.88	0.62
17	20.29	1.70	22	18.55	1.04	12	20.83	0.76
18	18.78	0.49	23	19.55	0.63	13	21.17	−0.14
20	21.39	0.26	24	21.38	−0.07	14	21.38	0.30
22	20.79	−0.03	25	21.81	1.33	15	19.12	1.19
23	20.75	0.02	26	20.86	1.58	16	22.19	0.29
24	19.83	0.85	27	21.52	−0.36	17	22.03	0.47
25	21.41	0.27	28	20.94	−0.08	18	19.64	1.28
26	17.87	0.92	30	19.76	0.60	19	18.82	0.58
27	18.06	1.07	31	18.06	1.10	20	20.67	1.63
29	20.13	0.53	32	18.75	1.06	21	22.19	0.21
31	19.64	1.54	III 3	22.20	0.27	22	19.93	0.75
32	19.27	0.79	4	21.29	0.95	23	18.93	0.51
33	21.20	−0.01	5	21.73	0.72	24	21.38	0.88
34	20.55	0.80	6	20.59	0.40	25	21.92	0.57
35	18.62	1.06	7	19.29	0.84	26	21.91	0.45
36	21.54	−0.19	8	17.68	0.37	27	21.86	0.60
37	21.28	0.84	9	21.72	0.75	28	21.84	0.51
38	18.57	1.45	11	19.70	1.21	29	20.62	0.84
40	20.56	1.33	12	17.10	0.49	30	21.95	0.54
41	19.05	1.39	13	19.22	0.84	31	20.55	1.33
43	21.15	0.12	14	21.09	1.61	32	20.68	0.70
44	21.83	0.13	15	20.71	1.13	33	19.12	0.33
45	21.54	0.23	17	18.04	0.70	34	21.06	0.94
46	20.83	0.76	18	21.37	0.97	35	20.63	0.68
47	21.84	0.12	19	20.67	0.67	36	21.70	0.75
49	21.26	0.49	20	22.11	0.03	37	21.64	0.80
50	21.05	0.76	21	19.20	1.52	38	20.39	0.14
51	19.93	0.76	22	19.23	1.30	39	19.32	0.89
52	20.82	1.09	23	20.78	0.00	40	17.33	1.42
53	19.94	0.66	24	20.56	0.62	41	19.39	0.80
54	21.16	0.45	26	21.15	1.08	42	21.18	1.19
55	21.43	−0.22	27	21.15	0.80	43	21.57	0.80
II 1	21.80	0.58	28	19.91	0.88	44	19.24	0.78
3	18.73	0.65	29	20.50	0.14	47	21.08	1.41

Table 4 presents the final list of V and $B - V$ values for the 700 photographically measured program stars. The internal random errors of the tabulated values, determined from the plate-to-plate residuals, are listed in table 5.

Plate-to-plate comparison of the faint-magnitude scales indicates that the final magnitude calibration should have a *systematic* error of less than ± 0.07 mag at $V \simeq 21$. Systematic errors in the *colors* of faint stars should be ± 0.05 mag or less; this is achieved by ensuring that the photographically determined colors of each primary-secondary image pair are the same (as they should be, since the "wedge" itself is achromatic).

Radial field errors were also investigated, by comparing the C-M arrays at varying distances from the cluster center. Corrections were found to be negligible except for faint stars ($V > 20$) within 5′.2 of the cluster center. Corrections (reaching 0.20 mag in the innermost region at $V \simeq 21$) were applied to the magnitudes of these stars, but no *color* corrections were found necessary.

The final C-M diagrams for rings A and B and for all data combined are presented separately in figures 5*a*, 5*b*, and 6; these will be discussed in § V below.

TABLE 5

RANDOM ERRORS OF PHOTOGRAPHIC MAGNITUDES

V	σ_V	σ_B	σ_{B-V}
≤19..........	0.05	0.02	0.05
20..........	0.04	0.05	0.06
21..........	0.10	0.09	0.14
22..........	0.18	0.13	0.22

III. COMPARISON WITH BAADE'S m_{pg} SCALE

The photometric scale in NGC 2419 used in the previous work by Baade (1935) was established by three closely consistent photographic transfers to a faint standard sequence in SA 51. In SA 51, Baade himself had used the exposure ratio technique to extend a bright sequence, which was itself transferred from the North Polar Sequence (Seares, Kapteyn, and van Rhijn 1930).

In order to transform Baade's observations of the variables in NGC 2419 to the present B magnitude scale, his m_{pg} values and our B magnitudes for a number of his standard stars were compared. In addition, the bright Mount Wilson magnitudes in SA 51 were compared with Baum's (unpublished) photoelectric measurements, since Baade did not publish his extended faint sequence in SA 51. The results are shown in figure 3 and indicate that for faint stars the Mount Wilson scale is compressed with respect to the present B scale, and that the trend in SA 51 continues in NGC 2419 without a perceptible break. This shows that Baade's transfers were correct and that the error lay with the SA 51 photographic scale. For the magnitude range of interest in NGC 2419 ($17 < B < 22$) the two scales are adequately transformed by the linear relation

$$B = 1.35\, m_{pg} - 5.36\,. \tag{2}$$

In figure 3, the random scatter of ± 0.09 mag (A.D.) in m_{pg} is gratifyingly small. Baade's photometry has an internal probable error of ± 0.06 mag; this implies an external probable error of ± 0.07 mag for the present B magnitudes for $18 < B < 23$, in reasonable agreement with the random errors of ± 0.08 mag mentioned previously (table 5).

IV. REDDENING DETERMINATION

Six methods can be used to determine the foreground reddening of NGC 2419. These are discussed below in approximate order of decreasing accuracy.

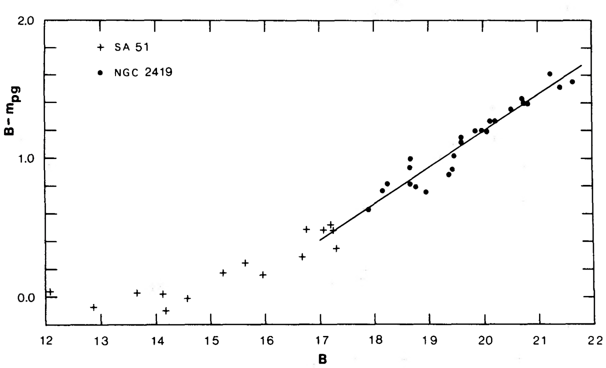

FIG. 3.—Comparison of the present B magnitude scale in NGC 2419 and in SA 51 with Baade's m_{pg} scale. The difference between the two scales, $B - m_{pg}$, is plotted as a function of B. For $B < 17$, Baum's photoelectric measures of stars in SA 51 are compared with the old m_{pg} values for these stars (Seares *et al.* 1918), and for $B > 17$, the plotted points are for Baade's (1935) standard stars in NGC 2419. The adopted relation between the two scales is given by eq. (2) in the text.

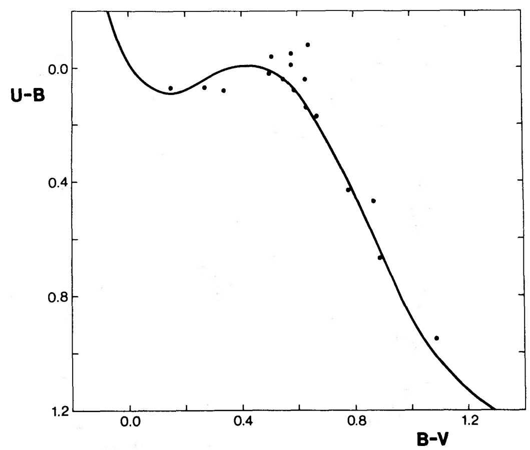

FIG. 4.—Two-color diagram for the photoelectric standard stars in table 1. All stars with at least three measurements in each color are plotted, along with the unreddened ZAMS line. A low foreground reddening of $E(B - V) \lesssim 0.04$ is indicated for NGC 2419.

a) *Integrated Color of Cluster*

Racine (1973) has calibrated the integrated color $(B - V)_0$ of a globular cluster in terms of its integrated spectral type (Kinman 1959*b*). The spectral type of F5 and integrated color $B - V = 0.68$ (Harris and van den Bergh 1974) lead to $E_{(B-V)} = 0.03$.

b) *UBV Photometry of Field Stars*

The two-color diagram for all the photoelectric standards in table 1 with at least three measurements in each color is shown in figure 4, together with the unreddened main sequence line. Neglecting the stars near $B - V = 0.6$ showing obvious ultraviolet excess, a reddening of $E_{(B-V)} \lesssim 0.04$ is derived.

c) *Blue Edge of RR Lyrae Gap*

The heavily populated blue horizontal branch seen in figure 5*a* stops abruptly at $B - V = 0.20 \pm 0.01$. The intrinsic color of this blue edge is assumed to be $(B - V)_0 = 0.17 \pm 0.01$ (Sandage 1969*a*), which implies $E_{(B-V)} = 0.03 \pm 0.02$. This method acts only as a check on the others, since it depends critically on the systematic accuracy of the photographic color determinations.

d) *Fitting to M92*

The C-M diagram for NGC 2419 is closely similar to that for the classical halo cluster M92 (Sandage 1970). Fitting the M92 ridge lines to the NGC 2419 diagram in figure 5*a* shows the latter to be redder by 0.02 ± 0.02 mag. Since M92 itself is reddened by 0.02 mag (Sandage 1969*a*), this implies $E_{(B-V)} = 0.04 \pm 0.02$ for NGC 2419.

e) *Reddening of NGC 2420*

The old open cluster NGC 2420 lies within 18° of NGC 2419 and at the same galactic latitude. An

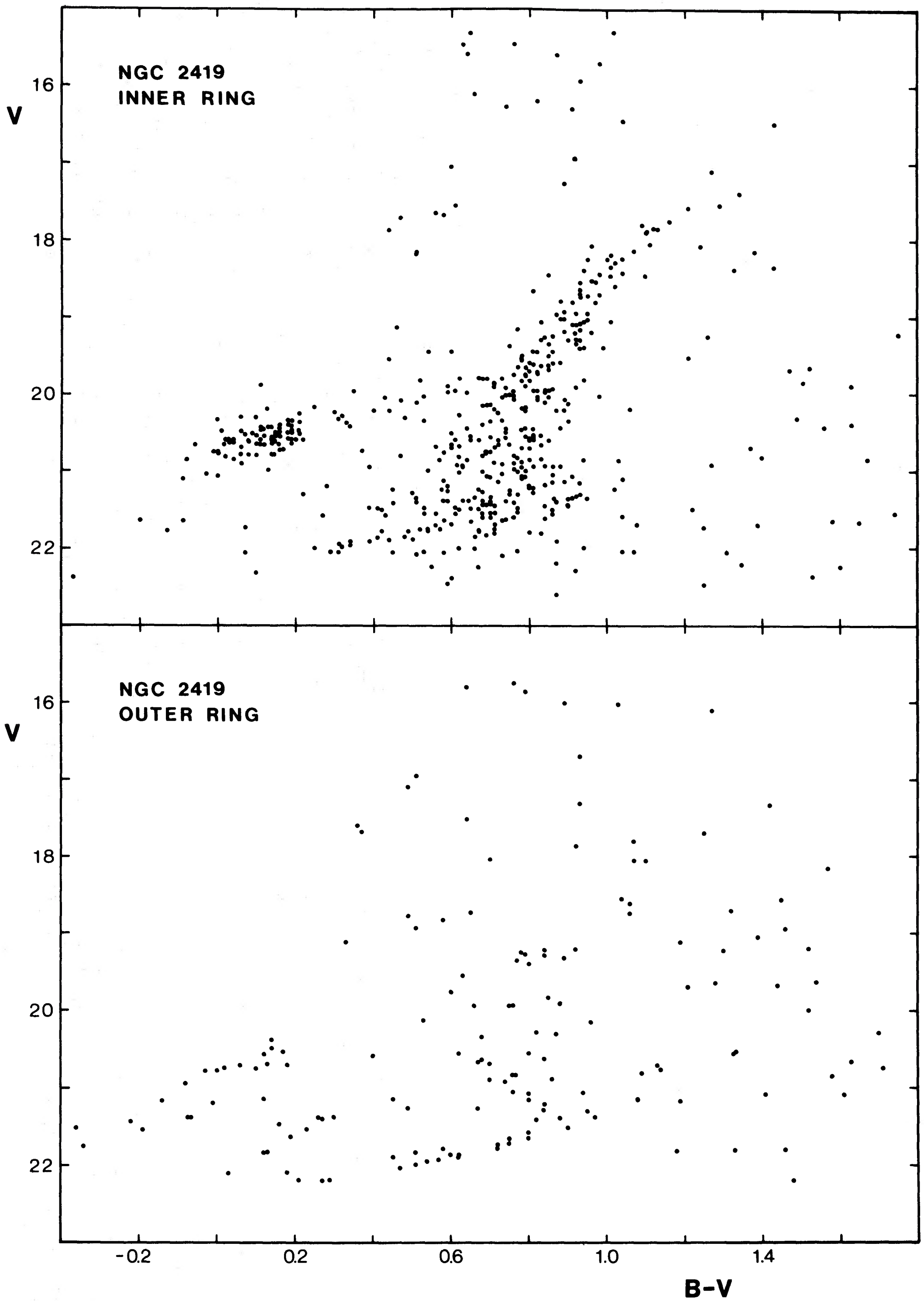

FIG. 5.—(*a*) C-M diagram for all measured stars in ring A, is listed in tables 1 and 4. (*b*) Same for the outer ring B. The population of foreground field stars should be the same for both rings since they have the same area.

TABLE 6

REDDENING DETERMINATIONS FOR NGC 2419

Method	$E(B-V)$
Integrated color..........	0.03
Field stars...............	0.04
RR Lyrae blue edge......	0.03
Fitting to M92...........	0.04
NGC 2420..............	0.02
Cosecant law............	0.04
Adopted mean	0.033 ± 0.01

intermediate-band and BV photometric study by McClure, Forrester, and Gibson (1974) yields $E_{(B-V)} = 0.02, \pm 0.01$ for NGC 2420.

f) *Cosecant Law*

The newly modified cosecant absorption law by Sandage (1973) predicts $E_{(B-V)} = 0.04$ at the galactic latitude of NGC 2419.

The various reddening estimates—which are remarkably consistent—are summarized in table 6. A final mean of $E_{(B-V)} = 0.033 \pm 0.01$ is adopted, corresponding to $A_V = 3.2E_{(B-V)} = 0.10 \pm 0.03$.

V. THE C-M DIAGRAM

a) *Morphology*

The C-M diagram displayed in figure 5*a* shows immediately that NGC 2419 has the characteristics of a "normal" halo globular cluster. The giant branch (GB), which sets in at $V \simeq 17.4$, $B - V \simeq 1.4$, has the steepness and color typical of metal-poor clusters, and a heavily populated blue horizontal branch (BHB) appears at $V \simeq 20.5$. A thin line of stars at $V \simeq 20.1$, $B - V \gtrsim 0.4$, may represent an incipient red horizontal branch, or the lower part of an asymptotic giant branch (AGB). Unfortunately the random errors in $B - V$ are too large to trace a possible AGB much higher than this.

The GB continues downward to the plate limit past $V \sim 22.3$. The data become incomplete below $V = 21.0$ in the inner part of ring A, where radial field errors also become noticeable. Foreground field stars appear to contribute about half the total population of the outer ring B, but these do not present a problem in ring A where the principal cluster sequences are well populated.

Figure 6 displays the combined C-M data for *all* stars in tables 1 and 4, along with some of the known variables (see § V*f* below); the mean ridge lines for this graph are given in table 7. It should be emphasized that figure 6 does *not* represent a homogeneous sample of data (as do figs. 5*a* and 5*b*), since the upper part of the giant branch has been reinforced by including the extra "inner region" stars.

b) *Metallicity*

Comparison with a number of other halo clusters shows that the NGC 2419 C-M diagram closely resembles those of the two classic very-metal-poor

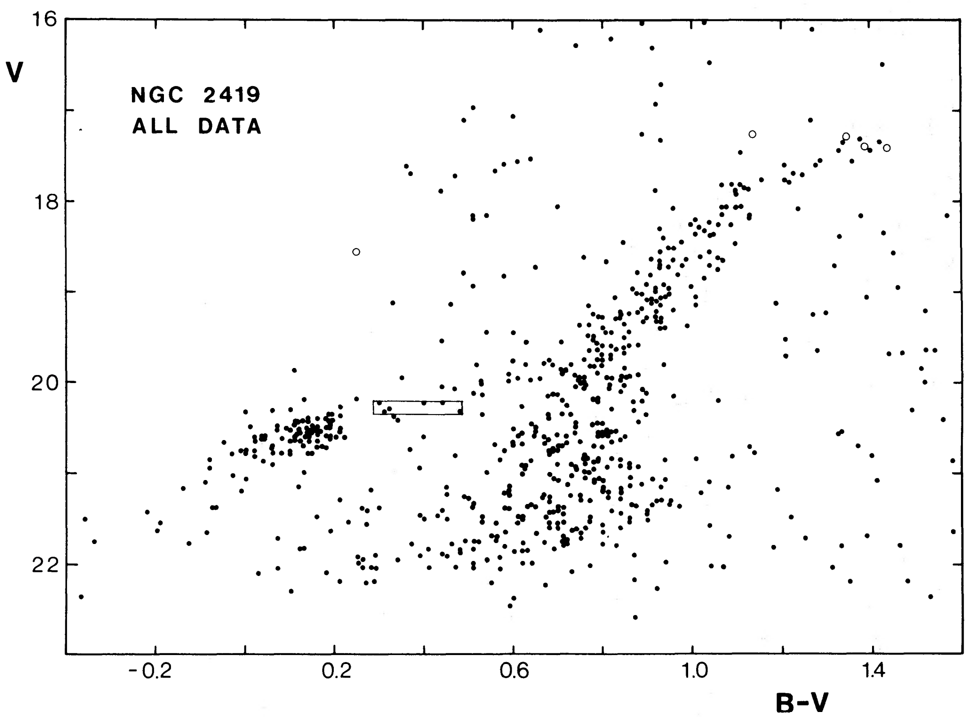

FIG. 6.—Combined C-M diagram for *all* measured stars, including the "inner region" as listed in table 4. The approximate mean positions of the five bright variables are shown by open circles, and the rectangular error box at $V \simeq 20.3$ denotes the mean position of the 12 short-period (RR Lyrae) variables measured in the present study.

TABLE 7

RIDGE LINES FOR COLOR-MAGNITUDE DIAGRAM

GIANT BRANCH		AGB + HB	
V	$B-V$	V	$B-V$
17.33	1.42	19.00	0.85
17.36	1.40	19.22	0.80
17.52	1.30	19.48	0.75
17.71	1.20	19.70	0.70
18.00	1.10	19.88	0.65
18.45	1.00	19.95	0.60
19.03	0.90	20.10	0.50
19.33	0.85	20.20	0.44
19.72	0.80	20.50	0.20
20.28	0.75	20.60	0.10
21.10	0.70	20.70	0.05
22.00	0.65	20.87	0.00
		21.00	−0.04
		(21.30	−0.10)
		(21.55	−0.15)

clusters M92 and M15 (Sandage 1970). The giant branch (GB) and blue horizontal branch (BHB) match extremely well with M92 in particular.

The low metallicity of NGC 2419 is further established by three well-known parameters describing the height and slope of the giant branch: the height ΔV at $(B-V)_0 = 1.4$ (Sandage and Wallerstein 1960), the intrinsic color at the level of the horizontal branch $(B-V)_{0,g}$ (Sandage and Smith 1966) and the slope S (Hartwick 1968). These are listed for NGC 2419 in table 8, in comparison with M92 and M15 (Sandage 1970).

One other notable feature in the C-M diagram of figure 6 is the way that the BHB cuts off abruptly at $V = 20.9$ with only a thin scattering of stars below this—again, resembling a similar phenomenon in M15 (Sandage, Katem, and Kristian 1968). This cannot be a result of incompleteness or selection effects, since it occurs even in the outer parts of ring A where these problems do not appear until $V > 21.5$. This cutoff may possibly be related to the "gap" discussed by Newell (1973), at $(B-V)_0 = -0.13$, $(U-B)_0 = -0.40$, in the distribution of field BHB stars.

c) *Distance*

The distance modulus of NGC 2419 can be estimated either from the level of the BHB and RR Lyrae variables, or by fitting to the M92 C-M diagram. For the latter method, NGC 2419 is 5.32 mag fainter than M92 as shown in § IV above. Combining this with $(m-M)_v(\text{M92}) = 14.63$ (Sandage 1970) then gives $(m-M)_V = 19.95$ for NGC 2419.

TABLE 8

PARAMETERS OF THREE METAL-POOR CLUSTERS

Parameter	M15	M92	NGC 2419
ΔV	3.2	3.2	3.15 ± 0.1
$(B-V)_{0,g}$	0.68	0.68	0.70
S	6.9	5.7	6.8 ± 0.5

For the horizontal branch, the stars in figure 6 at the blue edge of the RR Lyrae gap ($0.1 < B-V < 0.2$) fall at a mean level $\langle V\rangle_{\text{HB}} = 20.54 \pm 0.40$ (s.e.). This gives $(m-M)_V = 19.94$, assuming $M_V(\text{HB}) = 0.6$ (Sandage 1970).

Finally, the mean magnitude of the RR Lyrae variables can be used. Transforming Baade's mean m_{pg} for his 31 variables by equation (2) gives $\langle B\rangle_{RR} = 20.62 \pm 0.02$, or $\langle V\rangle_{RR} = 20.32 \pm 0.05$ assuming $\langle B-V\rangle_{RR} = 0.3 \pm 0.05$. By comparison, our own measurements of 12 of these stars from the B and V plates taken in a single 2-hour period, yield $\langle V\rangle_{RR} = 20.28 \pm 0.10$ (s.e.) and $\langle B-V\rangle_{RR} = 0.39 \pm 0.13$. This reinforces Baade's result and supports the identification of these stars as RR Lyrae types.

The difference of 0.22 ± 0.06 mag between the levels of the blue edge and of the RR Lyrae themselves is significant and suggests that the "horizontal branch" of NGC 2419 in fact slopes upward as $B-V$ increases. The thinly populated *red* horizontal branch noted previously in figure 6 thus seems to be a direct natural continuation of this slope; at $B-V = 0.6$ the HB is 0.5 mag higher than at the blue edge. This somewhat unusual feature of NGC 2419 will be rediscussed in the next section.

The distance modulus estimates are summarized in table 9, and lead to the adopted result $(m-M)_V = 19.87 \pm 0.09$ m.e., or $(m-M)_0 = 19.77 \pm 0.1$ with the adopted reddening (§ IV). [The quoted errors neglect the uncertainty in $M_V(\text{HB})$.] The result places NGC 2419 a distance of 90 ± 5 kpc from the Sun and 100 kpc from the Galactic center, more distant than any other known cluster. The immensity of this distance can be emphasized by noting that the brightest giant-branch stars in NGC 2419 are almost a full magnitude *fainter* than the main-sequence turnoff stars in the *closest* known globular cluster, NGC 6397 (Woolley *et al.* 1961)!

d) *Age*

A detailed comparison of the C-M diagram of NGC 2419 with theoretical models would be premature in view of the work in progress by a number of authors on the advanced evolution of globular-cluster stars. Nevertheless, a few brief comments can be made here on the age and abundance characteristics of NGC 2419 by referring to recent work by Rood (1973, 1974), who has been able to show how the morphology of the HB depends on cluster metallicity and age. Especially relevant to the case of NGC 2419 is Rood's finding that for very metal-poor clusters ($Z \sim 10^{-4}$) the HB indeed slopes up toward its red end. (For example, compare our fig. 6 with Rood's 1973 fig. 4*b*.) Since the HB slope (at constant Z) is nearly independent of age, this criterion can be used to estimate Z. Comparing Rood's models with the NGC 2419 C-M diagram, we estimate $Z \simeq 1.5 \times 10^{-4}$ for NGC 2419, confirming quantitatively our earlier conclusion about its very low metallicity. The age itself follows from the relative number of stars at the blue and red sides of the RR Lyrae region and from the way that the BHB extends to fainter magnitudes.

TABLE 9

DISTANCE MODULUS OF NGC 2419

Method	Assumptions	$(m - M)_v$
Blue edge of HB........	M_v (blue edge) = +0.6	19.94
Median B_{RR}............	M_v(RR) = +0.6	19.72
Fit to M92.............	Identical ridge lines; $(m - M)_{v,M92} = 14.63$	19.95
Adopted mean........		19.87 ± 0.09 m.e.
$(m - M)_0$...........		19.77 ± 0.10
Distance.............		90 ± 5 kpc

Again comparing NGC 2419 with Rood's models, we find $T = 11 \pm 0.5 \times 10^9$ yr. Note, however, that the *luminosity* of the HB in Rood's models is a sensitive function of the arbitrarily adopted mean mass loss in the pre-HB phases, and that his HB's are from 0.3 to 0.8 mag brighter than the "canonical" observational value $M_v = 0.6$ which we preferred to adopt for our distance estimate.

The age of NGC 2419 will be discussed again from a completely independent viewpoint in § VI, in relation to its galactic orbit.

e) Luminosity Function of the Giant Branch

Interest in the luminosity function of giant-branch stars in globular clusters was given new impetus by the work of Sandage *et al.* (1968), who pointed out the possible existence of "gaps" in the giant branch of M15 and other clusters. A similar analysis can effectively be carried out here for NGC 2419 because of the large number of stars measured. Visual inspection of figures 5*a* and 6 indicates a rather obvious "gap" at $V \simeq 20.3$, and two other noticeable ones at $V = 19.5$ and $V = 18.9$.

A simple statistical test of the significance of these possible gaps can be carried out in the manner employed by Hawarden (1971) and Newell (1973). Figure 7 shows the cumulative luminosity function for the giant branch of NGC 2419, where $N(V)$ is the total number of giants brighter than magnitude V. In this graph, a "gap" will appear as a horizontal break or flattening of the integral curve. The statistical significance can then be estimated by averaging the mean slopes of the curve on either side of the chosen gap, and using this average slope to predict the number N_0 of stars that would be expected to fall in the gap. Comparing N_0 with the actual number of stars N in the gap then gives the statistic $\chi^2 = (N_0 - N)^2/N_0$, from which the probability P of its chance occurrence can be evaluated (cf. the discussion by Newell 1973).

For the luminosity function in figure 8, the "gaps" at $V = 18.9$ and 19.5 prove to be not statistically significant ($P = 0.07$ and 0.12, respectively). The feature centered at $V = 20.3$ and 0.3 mag wide has $\chi^2 = 7.04$, from which $P = 0.008$. This gap must therefore be considered likely to be a physically significant feature, in the sense that it represents a temporary speeding up of stellar evolution through this region.

Another possible but more prosaic explanation of this feature might be that the C-M diagram has a well-populated asymptotic giant branch (AGB) which stops at $V \simeq 20.1$ just at the red horizontal branch, thus creating the illusion of a gap immediately below. For example, if we assume that one-third of the stars above the HB are part of a populous AGB, the gap would be significant at the 93 percent confidence level; but in this case, the *change* in slope at $V = 20.3$ in figure 8 would become significant.

It is notable that this gap is $\lesssim 0.2$ mag above the horizontal branch, whereas in the M15 data of Sandage *et al.* the principal gap is 0.9 mag above the horizontal branch. Theoretical suggestions made to explain the existence of a gap include the effects of interior rotation on the outward movement of the hydrogen-burning shell of a giant star (Demarque, Mengel, and Sweigart 1972), or simply fluctuations in the cluster's initial mass function (Iben 1971). In neither case is it clear whether any gap would be expected to occur always at the same point. Further work of this type on other clusters will be essential if the gap position is to be related to other cluster properties.

f) The Bright Variables

In addition to 31 short-period variables, Baade discovered five brighter variables which he believed to be irregular and to "probably belong to spectral types G to K." All but one of these are too close to the cluster's center to be measured by iris photometry. Their colors were therefore estimated visually on the two V and three B plates taken on 1972 March 9 and 10. The results are given in table 10 where $\langle V \rangle$ has been obtained by transforming Baade's median m_{pg} into $\langle B \rangle$, then applying the mean $\langle B - V \rangle$ estimates. These variables are shown as open circles in the C-M diagram of figure 6. V1, V8, and V20 are seen to fall at the tip of the GB. Notably, they occur at somewhat

TABLE 10

OBSERVATIONS OF BRIGHT VARIABLES

Variable	$\langle V \rangle$	$\langle B - V \rangle$
V1........	17.41	+1.44
V8........	17.30	+1.35
V10........	17.27	+1.14
V18........	18.57	+0.25
V20........	17.39	+1.39

1975ApJ...196..413R

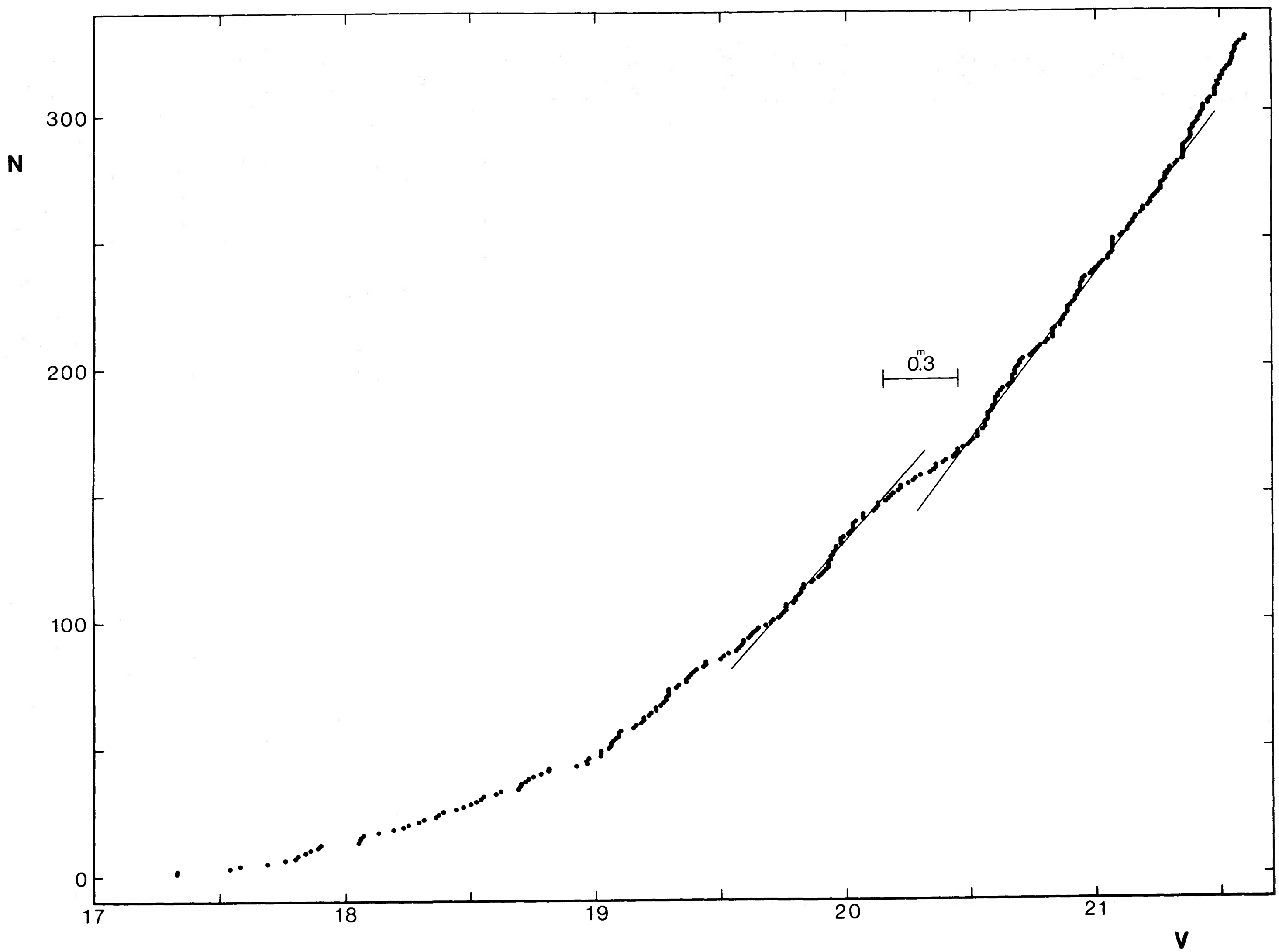

FIG. 7.—Cumulative luminosity function for the giant branch down to $V \simeq 21.5$. Here N is the total number of giant stars brighter than magnitude V, plotted as a function of V. All stars in rings A and B which fall on the giant branch are used.

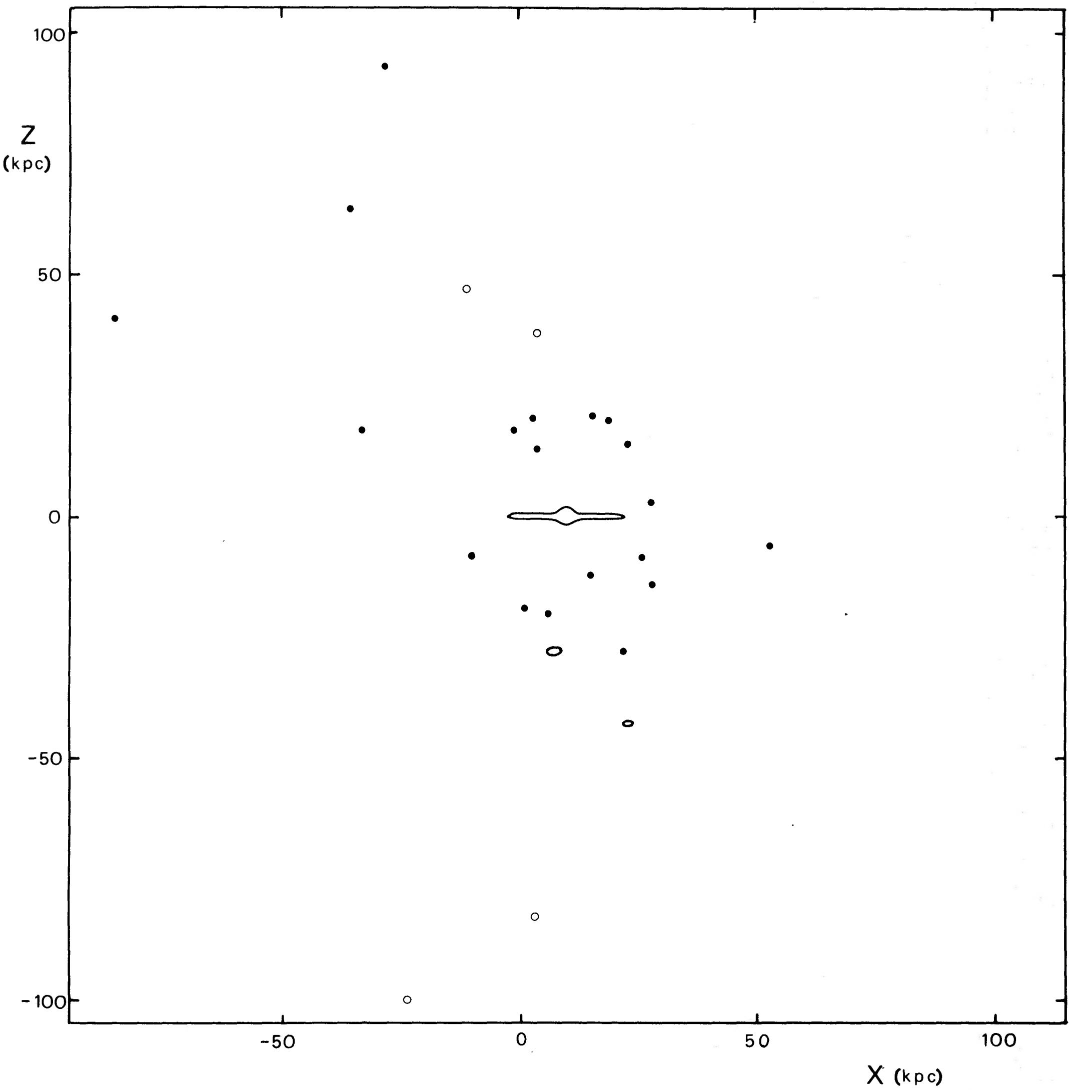

FIG. 8.—The distribution of "outer halo" objects, projected in the (X, Z)-plane. The diagram includes all objects with known galactocentric distances larger than 20 kpc. The Galactic disk is seen at center. Globular clusters are plotted as dots; dwarf spheroidal galaxies, as open circles; and the Magellanic Clouds, as the two small ellipses below the Galactic plane. NGC 2419 is the cluster at farthest left; this emphasizes its extreme distance and its present position at the fringe of the outer halo.

higher effective temperatures than the M-type variables found in later type globular clusters. Stothers (1963) points out that clusters rich in RR Lyrae variables tend to have shorter period and bluer late-type variables and the F3- to F5-type globulars produce RV Tauri variables. This appears to be confirmed in NGC 2419 whose integrated spectral type is F5 (Kinman 1959*b*). V10, slightly to the blue of the GB, is possibly an RV Tauri type.

The nature of the blue bright variable V18 is uncertain. Its position in the C-M diagram is too blue to be consistent with the location of the Population II Cepheid instability strip (Demers and Harris 1974); but its photometry is very uncertain, and a final conclusion must await a study of its light and color curves.

VI. ORBITAL KINEMATICS

a) The Outer Galactic Halo

Figure 8 shows the distribution of objects in the outer galactic halo (those with galactocentric distances greater than 20 kpc), projected on the (X, Z)-plane. NGC 2419 is seen to belong to the outermost fringes of our stellar system, comparable with the dwarf spheroidals and more distant than the Magellanic Clouds. In a forthcoming paper (Racine 1975) it will be shown that the galactic halo has an outer limiting radius R_t (imposed by tidal encounters with M31?) which falls in the range $8R_0 < R_t < 15R_0$, where the solar galactocentric distance is $R_0 = 9$ kpc (van den Bergh 1971). Hence the outlying systems in figure 8 may all be within R_t. Whether they are all actually gravitationally bound to the Galaxy might only be decided on the basis of their generally unavailable radial velocities.

A number of statistical investigations of the orbits of globular clusters have been published. Edmondson (1935) and Kurth (1960) found that the orbits (assumed to be ellipses) have axial ratios close to unity ($b/a > 0.8$), whereas von Hoerner (1955) and Kinman (1959*c*) concluded that the orbital eccentricities are high ($e > 0.8$). Because of the uncertainties involved in such studies, these two conclusions need not be incompatible; for an elliptical orbit, we have $b/a = (1 - e^2)^{1/2}$, and so $b/a \sim 1$ even for large eccentricities.

The picture of halo objects having highly eccentric orbits gained considerable substance from the classical study of the kinematics of nearby stars by Eggen, Lynden-Bell, and Sandage (1962, denoted ELS). They concluded, by studying a large sample of stars of different velocities and abundances, that the metal-poor galactic halo collapsed on a time scale comparable to the present rotation period of the disk ($\simeq 2 \times 10^8$ yr at the Sun). More recently this view has been challenged, particularly by Rood and Iben (1968) and Bond (1970) (but see footnote in Sandage 1970). In addition, Larson (1974) has provided strong evidence that the collapse phase and star-formation period of a large galaxy can be 10^9 years or longer even for the halo.

Conclusive evidence on the kinematics prevailing during the formation period of the present halo objects would be better obtained from a study of objects *now* in the halo, rather than from a sample of nearby stars selected on kinematical grounds. In practice, this approach is extremely difficult since the orbital parameters of these distant objects must be determined without knowledge of their tangential velocities. Large uncertainties may also be introduced by a possible error in our estimate of the circular velocity at the Sun. In the case of NGC 2419, however, the orbit *can* be uniquely determined.

b) *Orbital Parameters of NGC 2419*

Because NGC 2419 is so distant and lies in the anticenter direction, the angular separation between the Sun and the galactic center is only 2°.5 as seen from the cluster. Its radial velocity with respect to the Sun can thus be taken as the radial component V_R of its orbital velocity about the galactic center. Its measured radial velocity is $+14 \pm 20$ km s^{-1} (Kinman 1959*a*); after correcting to the local standard of rest (Delhaye 1965), this gives $V_R = +4 \pm 20$ km s^{-1}. Since V_R is essentially zero compared with the circular velocity at its present distance ($\Theta_c = 85$ km s^{-1} at 100 kpc, from Schmidt 1965), the cluster can therefore be assumed to be at either apogalacticon or perigalacticon.

Star counts in NGC 2419 (Peterson and King 1973) show that the cluster possesses a well-defined tidal radius of 10′. From this, Peterson (1974) deduces that the cluster must have a perigalacticon of $R_p =$ 22.5 kpc, using $R_g = 80$ kpc for its present galactocentric distance, and assuming a mass-to-light ratio within the cluster of unity. The new distance of $R_g = 100$ kpc determined here leads to $R_p = 24$ kpc. This then implies that NGC 2419 is gravitationally bound to the Galaxy, and is now very close to its apogalacticon.

TABLE 11

Orbital Parameters for NGC 2419*

Semimajor axis	62 kpc
Eccentricity	0.62
Period	3.4×10^9 yr
Time of perigalacticon passage	1.7×10^9 yr ago

* Adopted galactic mass: $1.8 \times 10^{11} M_\odot$ (Schmidt 1965).

The orbital parameters, derived under the assumption of an elliptical orbit, are summarized in table 11. The orbit is completely determined *except* for inclination and sense of rotation; for no other cluster is it possible to do this, either because the geometry is ambiguous or the radial velocities are unknown. It should be emphasized that the parameters in table 11 are rather insensitive to the detailed mass model of the Galaxy and (except for the eccentricity) depend only weakly on the value of R_p derived from the tidal radius. This is so because, for most or all of its orbit, NGC 2419 is at such a huge galactocentric distance that only the *total* mass M_g of the Galaxy affects its motion. In particular, the time elements in table 11 scale as $M_g^{-1/2}$.

c) *Angular Momentum of Halo Clusters*

Although the present orbit of NGC 2419 may not be its original one (§ VI*d* below), it must at present possess a high angular momentum h per unit mass, since it moves on such a large orbit of axial ratio $b/a = 0.8$. This is contrary to the ELS picture of old halo objects moving in "nearly rectilinear orbits" of low h, and suggests that it would be worthwhile to compare this feature of NGC 2419 with the other globular clusters.

Peterson's (1974) recent determination of perigalacticon distances R_p for 41 clusters can be used to compute *minimum* values of h for these clusters, from the general relation

$$h^2 = GMR_p(1 + e) . \qquad (3)$$

On the other hand, the *maximum* possible value of h for each cluster can be found by assuming $e = 1$. The frequency distributions of $h_{\min}$ and $h_{\max}$ are shown in figure 9, where h has been normalized to the mass-weighted mean angular momentum for the Galaxy according to the Schmidt (1965) mass model. For the Sun, $h \simeq \langle hg \rangle = 2500$ km kpc s^{-1}. It is apparent from the figure that the *outer halo* clusters possess orbital angular momenta which are generally *larger* than those of the clusters close to the galactic disk. Furthermore, figure 10 shows how h correlates with the metallicity parameter Q (van den Bergh

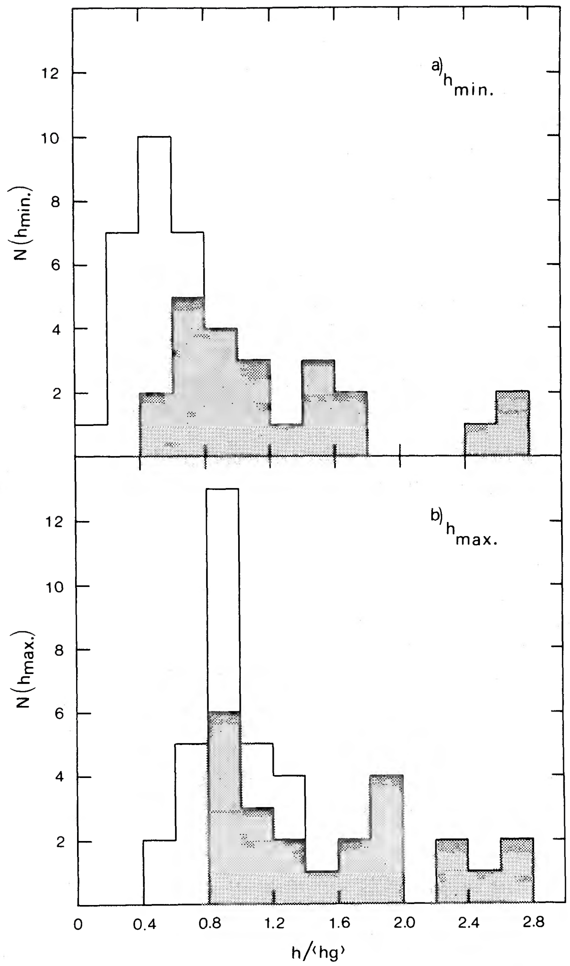

FIG. 9.—(*a*) Frequency distribution of the angular momentum per unit mass *h* for globular clusters, assuming minimum orbital eccentricity. The group of halo clusters (R_g > 10 kpc) are plotted as grey strips. (*b*) Same distribution assuming maximum possible orbital eccentricity, $e = 1$. The figure shows that the halo clusters tend to have more angular momentum than the inner "disk" clusters.

1967) for globular clusters. This reveals that the clusters with the largest angular momenta are among the metal-poorest.

The statement made by ELS—namely, that the old, metal-poor halo objects have orbits of high eccentricity and low angular momentum—clearly differs from the conclusion drawn here. Figures 9 and 10 demonstrate that those objects *in the halo now* were born from protogalactic material, which, at their formation time, *already* had a substantial amount of angular momentum. Furthermore, since so many extremely metal-poor clusters have high *h*, this proto-cluster material possessed this angular momentum *before* metal enrichment took place.

It should be stressed that our conclusions modify those of ELS because the objects used here differ fundamentally from theirs. The sample analyzed by ELS consisted of stars of all *different* ages, abundances, and velocities, but was inevitably restricted to stars now in the local solar neighborhood. The old metal-poor stars in this selected sample thus have orbits of predominantly *low* angular momentum with apogalactica near the Sun, and few stars are seen with large orbits taking them well beyond the Sun. By contrast, the globular clusters discussed here are *all* extremely old objects in the sense that they belong to the earliest phase of the Galaxy, and they are spread out in a vast region throughout the halo. Not surprisingly, many of these have large orbits of *high* angular momentum and small or moderate eccentricity, and represent a kinematic class of extremely old objects not seen by ELS in their sample. Notably, later work by Sandage (1969*b*) showed that indeed, old stars with these characteristics can be found even near the Sun. The principal conclusion here is that objects in the halo, which were formed during the initial collapse phase of the Galaxy, could be formed in orbits of *any* shape and angular momentum.

It should be pointed out that in the angular momentum statistics discussed here, as in ELS, the sign of *h* is neglected. For globular clusters, nothing else can be done since the sense of the orbits is generally unknown. For nearby high-velocity stars with accurate astrometric data, Eggen and Freeman (private communication) find that direct and retrograde orbits have significantly different distributions of angular momenta. It would be very exciting if a similar analysis for globular clusters could be carried out! (We are indebted to Professor Eggen for bringing this point to our attention.)

d) *The Origin of NGC 2419*

Since NGC 2419 is by its morphology and its C-M diagram so similar to the "inner" halo objects (R_g < 20 kpc), and so different from objects in its own spatial "neighborhood" at $R_g \sim 100$ kpc, it may therefore be logical to suggest that the cluster was formed while close to its perigalacticon distance, at a time and place where the other inner halo objects were born. If the cluster's orbit has remained essentially unperturbed since its birth, an unorthodox but amusing estimate of its age could be based on the times of perigalacticon passages computed from the orbital data of table 11. And since the cluster *remains* near its perigalacticon in the inner halo (R_g < 50 kpc) for less than 0.6×10^9 yr, the birth date thus found would be accurate to $\pm 0.3 \times 10^9$ yr if the correct passage were identified. Tracing the orbit backward suggests that possible epochs of formation are 8.5, 11.9, and 15.3×10^9 yr ago. Current estimates of the absolute ages of globular clusters (Iben and Rood 1970*a*, *b*; Rood 1970, 1973; Sandage 1970; Demarque, Mengel, and Aizenman 1971; Demarque *et al.* 1972) range between 10×10^9 yr and 13×10^9 yr. This would favor $T = 11.9 \pm 0.3 \times 10^9$ yr for NGC 2419. The agreement between this value and $T = 11 \times 10^9$ yr found in § V from the HB morphology is comforting but probably fortuitous.

The weakness of the above argument stems from the assumption of an unperturbed orbit. The very fact

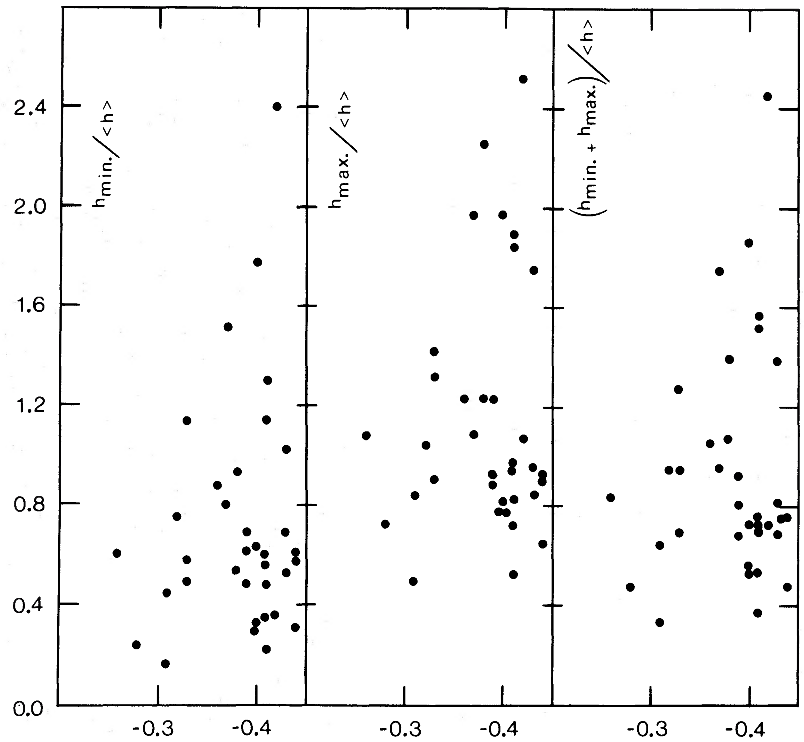

FIG. 10.—Relation between the metallicity parameter Q and the (a) minimum, (b) maximum, and (c) median angular momentum per unit mass, for 35 globular clusters. Clusters with the largest values of h tend to have low metallicity.

that NGC 2419 has so many family traits of the inner halo objects might be taken to mean that the cluster was "launched" from a lower initial orbit by a gravitational encounter with a more massive object, possibly one of the Magellanic Clouds. Rough calculations show that the probability of at least one halo cluster being significantly perturbed by a Magellanic Cloud passage (as proposed by Toomre 1972) is relatively high. In this event our results on the orbit of NGC 2419 could help to define further constraints on the geometry of such a Cloud-Galaxy encounter. In particular, if such an encounter is responsible for the present orbit of NGC 2419, the Magellanic Cloud(s) must be gravitationally bound to the Galaxy, because the last perigalacticon passage of NGC 2419 ($T \sim 1.7 \times 10^9$ yr ago) occurred long before the last passage of the Cloud(s) through the inner halo ($T \sim 0.5 = 10^9$ yr ago). This means that any encounter must have taken place on a previous passage of the Clouds.

VII. CONCLUSION

NGC 2419 is a normal, low-metallicity globular cluster presumably formed in the inner galactic halo. The cluster is gravitationally bound to the Galaxy, and its extremely large apogalactic distance and moderately low orbital eccentricity may be the result of the initial conditions at formation, but might also be due to an encounter with the Magellanic Clouds. Further studies of the Clouds' orbits guided by the present findings are needed to clarify this point.

The 31 short-period variables discovered by Baade are RR Lyrae-type from their position in the C-M diagram, and three of the five bright variables are red giants whereas the other two may be Cepheid or RV Tauri types. It is hoped that the magnitude sequences defined here in NGC 2419 will prove useful to the study of these variables.

A significant gap is observed in the red giant branch 0.2 mag above the HB. The gap position is different from that observed in other clusters.

Finally it is pointed out that the angular momentum per unit mass of the outer-halo globular clusters is generally large and that the conventional picture of very elongated plunging orbits for globular clusters may need revision.

We are greatly indebted to Dr. H. W. Babcock, Director, Hale Observatories and Dr. L. Goldberg, Director, KPNO, for the privilege of using the Palomar and Kitt Peak facilities and for generous allocations of observing time, without which this project could not have been completed. Correspondence with Dr. T. D. Kinman during the 4-year period since our first contact with NGC 2419 was instrumental in stimulating this research. Numerous discussions with and objections from Dr. S. van den Bergh and Dr. D. A. MacRae helped to put this paper into reasonable form.

Financial support through the National Research Council of Canada is gratefully acknowledged.

REFERENCES

Baade, W. 1935, *Ap. J.*, **82**, 396.
Baade, W., and Swope, H. 1961, *A.J.*, **66**, 300.
Bond, H. E. 1970, *Ap. J. Suppl.*, **22**, 117.
Burbidge, E. M., and Sandage, A. R. 1958, *Ap. J.*, **127**, 527.
Crawford, D. L., Golson, J. C., and Landolt, A. U. 1971, *Pub. A.S.P.*, **83**, 652.
Delhaye, J. 1965, in *Galactic Structure*, ed. A. Blaauw and M. Schmidt (Chicago: University of Chicago Press), p. 61.
Demarque, P., Mengel, J. G., and Aizenman, M. 1971, *Ap. J.*, **163**, 37.
Demarque, P., Mengel, J. G., and Sweigart, A. V. 1972, *Ap. J.* (*Letters*), **173**, L27.
Demers, S., and Harris, W. E. 1974, *A.J.*, **79**, 627.
Edmondson, F. K. 1935, *A.J.*, **45**, 1.
Eggen, O. J., Lynden-Bell, D., and Sandage, A. R. 1962, *Ap. J.*, **136**, 748 (ELS).
Harris, W. E., and van den Bergh, 1974, *A.J.*, **79**, 31.
Hartwick, F. D. A. 1968, *Ap. J.*, **154**, 475.
Hartwick, F. D. A., and McClure, R. D. 1972, *Ap. J.* (*Letters*), **176**, L57.
Hawarden, T. G. 1971, *Observatory*, **91**, 78.
Iben, I. 1971, *Pub. A.S.P.*, **83**, 697.
Iben, I., and Rood, E. T. 1970*a*, *Ap. J.*, **159**, 605.
———. 1970*b*, *ibid.*, **161**, 587.
Johnson, H. L., Mitchell, R. I., Iriarte, B., and Wisniewski, W. Z. 1966, *Comm. Lunar and Planet. Lab.*, **4**, 99.
Kinman, T. D. 1959*a*, *M.N.R.A.S.*, **119**, 157.
———. 1959*b*, *ibid.*, **119**, 538.
———. 1959*c*, *ibid.*, p. 558.
Kurth, R. 1960, *Zs. f. Ap.*, **50**, 215.
Larson, R. B. 1974, *M.N.R.A.S.*, **166**, 585.
McClure, R. D., Forrester, W. T., and Gibson, J. 1974, *Ap. J.*, **189**, 409.
Newell, E. B. 1973, *Ap. J. Suppl.*, **26**, 37.
Peterson, C. J. 1974, *Ap. J.* (*Letters*), **190**, L17.
Peterson, C. J., and King, I. R. 1973, *Bull. AAS*, **4**, 385.
Racine, R. 1969, *A.J.*, **74**, 1073.
———. 1971, *Ap. J.*, **168**, 393.
———. 1973, *A.J.*, **78**, 180.
———. 1975, in preparation.
Rood, R. 1970, *Ap. J.*, **161**, 145.
———. 1973, *ibid.*, **184**, 815.
———. 1974, preprint.
Rood, R., and Iben, I. 1968, *Ap. J.*, **154**, 215.
Sandage, A. R. 1969*a*, *Ap. J.*, **157**, 515.
———. 1969*b*, *ibid.*, **158**, 115.
———. 1970, *ibid.*, **162**, 841.
———. 1973, *ibid.*, **183**, 711.
Sandage, A. R., and Smith, L. L. 1966, *Ap. J.*, **144**, 886.
Sandage, A. R., and Wallerstein, G. 1960, *Ap. J.*, **131**, 598.
Sandage, A. R., and Wildey, R. 1967, *Ap. J.*, **150**, 469.
Sandage, A. R., Katem, B., and Kristian, J. 1968, *Ap. J.* (*Letters*), **153**, L129.
Schmidt, M. 1965, in *Galactic Structure*, ed. A. Blaauw and M. Schmidt (Chicago: University of Chicago Press), p. 513.
Seares, F. H., Kapteyn, J. C., and van Rhijn, P. J. 1930, *Carnegie Pub.*, No. 402.
Stothers, R. 1963, *A.J.*, **68**, 242.
Toomre, A. 1972, *Quart. J.R.A.S.*, **19**, 266.
van Agt, S. L. T. J. 1967, *B.A.N.*, **19**, 275.
van den Bergh, S. 1967, *A.J.*, **72**, 70.
———. 1971, *ibid.*, **76**, 1082.
von Hoerner, S. 1955, *Zs. f. Ap.*, **35**, 255.
Woolley, R. v. d. R., Alexander, J. B., Mather, L., and Epps, E. 1961, *R.O.B.*, No. 43, E303.

WILLIAM E. HARRIS: Yale University Observatory, P.O. Box 2023, Yale Station, New Haven, CT 06520
RENÉ RACINE: David Dunlap Observatory, Richmond Hill, Ontario, Canada, L4C 4Y6